

Stargardt Phenotype Associated With Two *ELOVL4* Promoter Variants and *ELOVL4* Downregulation: New Possible Perspective to Etiopathogenesis?

Luigi Donato,¹⁻³ Concetta Scimone,^{2,3} Carmela Rinaldi,³ Pasquale Aragona,³ Silvana Briuglia,³ Angela D'Ascola,³ Rosalia D'Angelo,³ and Antonina Sidoti^{2,3}

¹Department of Chemical, Biological, Pharmaceutical and Environmental Sciences, University of Messina, Messina, Italy

²Department of Cutting-Edge Medicine and Therapies, Biomolecular Strategies and Neuroscience, Section of Neuroscience-Applied

Molecular Genetics and Predictive Medicine, Istituto Euro Mediterraneo di Scienza e Tecnologia (I.E.M.E.S.T.), Palermo, Italy

³Department of Biomedical and Dental Sciences and Morphofunctional Imaging, University of Messina, Messina, Italy

Correspondence: Rosalia D'Angelo, Department of Biomedical and Dental Sciences and Morphofunctional Imaging, Division of Molecular Genetics and Preventive Medicine, University of Messina, via C. Valeria 1, I-98125 Messina, Italy; rdangelo@unime.it.

Submitted: September 11, 2017

Accepted: January 7, 2018

Citation: Donato L, Scimone C, Rinaldi C, et al. Stargardt phenotype associated with two *ELOVL4* promoter variants and *ELOVL4* downregulation: new possible perspective to etiopathogenesis? *Invest Ophthalmol Vis Sci*. 2018;59:843-857. <https://doi.org/10.1167/iops.17-22962>

PURPOSE. Stargardt disease (STGD) is the most common form of inherited juvenile macular degeneration. It is inherited as autosomal recessive trait (STGD1), although STGD3 and STGD4 are inherited as autosomal dominant inheritance pattern. STGD3 is caused by mutations in the elongation of very long-chain fatty acids-like 4 (*ELOVL4*) gene encoding for a very long-chain fatty acid elongase. Mutations lead to a truncated Elov14, lacking of a dilysine motif necessary for retention of transmembrane proteins in the endoplasmic reticulum. STGD occurs due to altered synthesis of very long-chain polyunsaturated fatty acids (VLC-PUFA). Our work investigates the role of two variants in the *ELOVL4* gene promoter region, c.-236 C>T (rs240307) and c.-90 G>C (rs62407622), identified in a patient with STGD in transconfiguration.

METHODS. Their effects on *ELOVL4* expression were examined by Dual-Luciferase Reporter assay.

RESULTS. rs62407622 and rs240307 variants caused 14% and 18% of expression reduction, respectively, compared with wild-type promoter. A very strong decreased gene expression was caused by coexistence of both variants.

CONCLUSIONS. A highly reduced activity of the *ELOVL4* promoter was registered due to combination of two variants. Decrease of *ELOVL4* enzymatic activity could lead to a deficiency of VLC-PUFA, essential components for rods function and longevity, which are among the parameters involved in the etiopathogenesis of STGD.

Keywords: Stargardt disease, macular degeneration, retinal degeneration, photoreceptors, VLC-PUFA

Stargardt disease (STGD) is a form of retinal dystrophy usually characterized by a progressive loss of central vision associated with irregular macular and perimacular yellow-white fundus flecks, and a so-called "beaten bronze" atrophic central macular lesion. Worldwide prevalence of STGD is estimated between 1/8000 and 1/10,000.¹

Typical disease onset does not exceed the twentieth year of life, although symptoms can also appear during adulthood and as late as the seventh decade.² Although disease severity and progression varies widely, STGD is usually characterized by loss of visual acuity, followed by wavy vision, blind spots, blurriness, impaired color vision, photophobia, and difficulty adapting in the dark.³

Today, three forms of STGD are known: STGD1, STGD3, and STGD4.⁴ STGD3 (Online Mendelian Inheritance in Man [OMIM] #600110) is a rare dominant form due to mutations in the elongation of very long-chain fatty acids-like 4 (*ELOVL4*) gene on chromosome 6q16.⁵⁻⁸ *ELOVL4* plays a fundamental role in the synthesis of very long-chain polyunsaturated fatty acids (VLC-PUFA).^{9,10} VLC-PUFA make up a considerable part of phosphatidylcholine (PC) in the outer segment of both cell types of photoreceptors, suggesting a relevant role in the

correct folding of disk rim and in cones and rods membrane fluidity.¹¹ These functions, together with a close interaction with rhodopsin, strongly point to the possible involvement of *ELOVL4* in phototransduction.¹² Furthermore, recently, VLC-PUFA have also been found in conventional synapses and retina ribbon, probably being incorporated into vesicles containing glutamate, in rods terminals.¹³

So far only nine *ELOVL4* variants are known: six single nucleotide and three indel/del mutations. Among these, four variants are in exon 6 and associated with the STGD3 form.¹⁴ According to this data, it would appear that Elov14 truncated protein loses the endoplasmic reticulum retention signal (KXKXX) and is mislocalized from the site of synthesis of VLC-PUFA. This condition leads to retina degeneration, due to: (1) production of toxic 3-keto-acylintermediates that imply cell death, and (2) reduced levels of VLC-PUFA and mislocalization of mutant protein, along with cellular stress, causing impairment of important cellular functions.⁵ It cannot be excluded that, in these situation, several chaperons, like HSP90, could help to solve the problem, as in other ocular diseases.¹⁵



Here, we report the case of a patient with dominant STGD in which we identified two *ELOVL4* promoter variants, c.-236 C>T (rs240307) and c.-90 G>C (rs62407622).

The effects of the single c.-90 G>C and c.-236 C>T variants, as well as two variants together ones (c.-90 G>C and c.-236 C>T) on gene expression and, consequently, on the onset of disease, were examined.

MATERIALS AND METHODS

Clinical Data

The proband, a 42-year-old Caucasian man, came to our attention with a diagnosis of STGD, showing visual problems since young age. His visual acuity was 1.6/10 in the right eye and 2/10 in the left eye; his peripheral visual field was well represented, while the central one was almost absent. Moreover, he also showed an initial loss of color vision, photophobia, and a slow dark adaptation. Diagnosis was the result of the following evaluations: fundus analysis, fundus autofluorescence (FAF), infrared reflectance imaging (IR), optical coherent tomography (OCT), visual field (VF), International Society for Clinical Electrophysiology of Vision (ISCEV) ERG, and pattern electroretinogram (PERG). Fundus examination revealed bilateral anisotropic, rounded maculopathy with sharp edges, surrounded by pisciform flecks, confirmed by IR and FAF (Fig. 1). Furthermore, FAF showed mottled areas of hyperautofluorescence and hypoautofluorescence, corresponding to areas of lipofuscin accumulation and RPE atrophy, respectively. ERG revealed a generalized rods dysfunction with cones involvement (photopic and scotopic hypovolted ERG), with a delay in visual response (PERG with hypovolted P50 wave and increased latency; BiomedicaMangoni, Pisa, Italy; Fig. 2). VF showed central scotoma correlating with outer retinal subfoveal atrophy observed on FAF and OCT (Fig. 3). In details, OCT highlighted disruption of both inner and outer photoreceptor segment layers, combined with the loss of the inner segment-outer segment junction and thinning of other retina layers.

The patient's family, composed of father and mother, was evaluated by the same clinical and instrumental analyses and resulted healthy. Both parents did not manifest bilateral central visual loss, photophobia, color vision abnormalities, central scotomas, or slow dark adaptation. Moreover, they showed a visual acuity of 20/20, a normal visual field, and a clean fundus.

We screened all three known STGD causative genes (*ABCA4*, *ELOVL4*, and *PROM1*), and we found no associated or causative variants (HGMD Professional was the most important and updated database we considered; Qiagen Aarhus Prismet, Aarhus, Denmark), except those we analyzed in this paper.

In order to evaluate the variants effects on *ELOVL4* expression, we performed a genetic analysis of the gene promoter through PCR and Sanger sequencing, followed by an in silico prediction and the functional Dual-Luciferase Reporter assay. The latter was essential to experimentally confirm the previously generated data.

Genotyping

DNA was extracted from leukocytes by using standard protocols. Amplification of regulatory regions of *ELOVL4* gene was performed using primer pairs designed according to the published nucleotide sequence of GenBank (accession no. NG_009108.1; available upon request).

The PCR mix was prepared by adding 8 µg of genomic DNA to 50 µL reaction mixture containing a 0.2 µM concentration of

each primer and 1 U MyTaq polymerase (Bioline, Aurogene Srl, Rome, Italy). PCR was carried out in the thermal cycler (Gene Amp PCR System 2700; PE Applied Biosystems, Foster City, CA, USA) under the following conditions: denaturation at 95°C for 15 seconds, annealing at 49.5°C for 15 seconds, and extension at 72°C for 10 seconds for 35 cycles, after an initial 1 minute denaturation at 95°C.

PCR products were sequenced by direct sequencing, using BigDye Terminator (ThermoFisher Scientific, Life Technologies, Monza, Italy) and Applied Biosystems 3500 Genetic Analyzer. The nucleotide number relative to variants identified in the promoter region of 805 bp was indicated in respect to the transcriptional start site of the reference sequence reported by the National Center for Biotechnology Information (NCBI) database. To name two polymorphisms we relied on Human Genome Variation Society (HGSV) nomenclature. Therefore, c.-90G> C (rs62407622) and c.-236C> T (rs240307) indicated nucleotide substitutions at RNA level.

In Silico Analysis

In silico analysis was performed on the *ELOVL4* promoter using two transcription factors (TF) prediction tools, individually and in pairs: BioBase TRANSFACTM Professional¹⁶ and Alggem PROMO.¹⁷ These tools were used to identify potential TF binding sites in the region where the variants in the *ELOVL4* promoter were found. TRANSFACTM was set to use the profile matrix for vertebrates, with a cutoff to minimize false positives (minFP). This is defined as the score that gives 1% of hits in the used sequences relative to the number of hits received at the minimum false negative (minFN) cutoff (the score at which at least 90% of the positive test set are recognized, i.e., it equals a false negative rate of 10%). The false positive rate is estimated by applying the Match algorithm (BIOBASE GmbH, Halchtersche, Wolfenbüttel, Germany) to upstream sequences.

PROMO, instead, involves the dissimilarity threshold; a parameter that controls how similar a sequence must be to the matrix to be reported as a hit. It was set at 15% (85% similarity). Random expectation (RE) gives the number of expected occurrences of the match, in a random sequence of the same length as the query sequence, according to the dissimilarity index. Two models are considered: (1) equiprobability for the four nucleotides (RE equally), and (2) estimate the nucleotide probability as the nucleotide frequencies in the query sequence (RE query).

Furthermore, Cytoscape software (The Cytoscape Consortium, New York, NY, USA) and its MCODE plug-in were used to analyze pathways between involved TFs, in order to predict possible interactions among them.

Cell Culture

U373 MG (human, Caucasian, glioblastoma-astrocytoma) cells (Sigma-Aldrich, Milan, Italy) were cultured in Dulbecco's modified Eagle's medium (DMEM) supplemented with 10% fetal bovine serum (FBS), 100 U/mL penicillin, and 1 mg/mL ampicillin (Lonza, Amboise, France) at 37°C in a water-saturated atmosphere with 5% CO₂. The essential feature that led us to choose this cell line was the acquisition of infinite growth potential, which set the stage for multiplication of genetic variants with an ever increasing fitness for proliferation and spread.

We used a glioblastoma cells line to perform another dual luciferase assay, involving cerebral cavernous malformations.¹⁸ This cell line can be useful because the retina has a nervous derivation as glia. Despite this, it is not possible to exclude that the whole transcription factors set in glioblastoma cells could be quite different from that in retina cells. In order to clarify

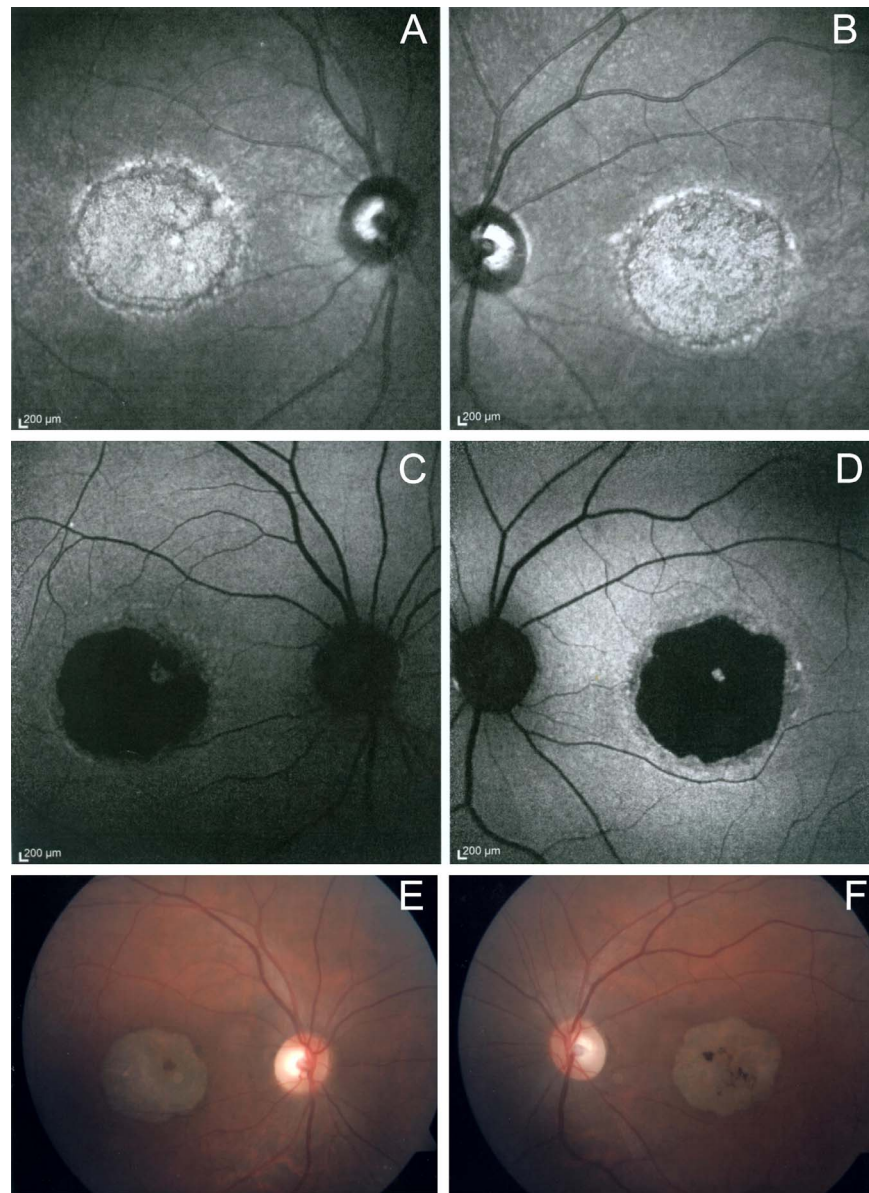


FIGURE 1. Infrared images (A, B), FAF (C, D), and fundus photograph (E, F), for the Proband compared with overt STDG3 (G–I) and control (J, K). Both *right* (C) and *left* (D) eyes show absence of FAF in the fovea, corresponding to geographic atrophy. Moreover, (A, B) evidence a central, bright, hyperreflective area, which corresponded to the atrophic macular lesion, surrounded by a darker, hyporeflective zone with distinct borders. This area is consistent with a zone where there is thinning and hypopigmentation of the RPE. This appearance is similar to established STDG3 in another patient, as evidenced in fundus photograph (G), fluorescein angiogram (H), and FAF (I). The fundus photograph and FAF of a healthy control are shown in (J, K).

this point, we address some supporting evidence: almost all TFs coming from our *in silico* analysis result expressed both in glioblastoma cells and retina cells, as evidenced by DPRP database,¹⁹ based on expression and ChIP-Seq experimental data, and TiGER.²⁰ Moreover, description of common TFs was reported among others also by Rheinbay et al.²¹ and Mysickova et al.²²

Construction of the Reporter Gene Plasmids

In order to highlight if the variants could affect *ELOVL4* expression, the effects of two combined genotypes, c.-236T/c.-90C (T-C) and c.-236C/c.-90C (C-C), on promoter activity were studied. An 805 bp promoter sequence was amplified by PCR using genomic DNA from the proband and one donor, selectively carrying each haplotype, using the following primers:

forward: 5'-AGATCTACATGCACCTTCTCTTGTC-3' and reverse: 5'-AAGCTTCACTACGTTTAGGACAC-3' under these conditions: 1 cycle of 95°C for 1 minute; 35 cycles of 95°C for 15 seconds, 49.5°C for 15 seconds, and 72°C for 10 seconds; and 1 cycle of 72°C for 7 minute.

Each PCR product, as well as pGL4.10 (*luc2*) was digested by *BglII* and *HindIII* (Promega Italia, Milan, Italy) and then purified (PureLink PCR Purification Kit; ThermoFisher Scientific, Life Technologies). Each promoter and pGL4.10 (*luc2*), digested and purified, was incubated overnight in appropriate concentrations, in order to execute ligation. The efficiency of promoter insertion upstream of the luciferase gene, cloned into the pGL4.10 (*luc2*), was verified by agarose gel electrophoresis.

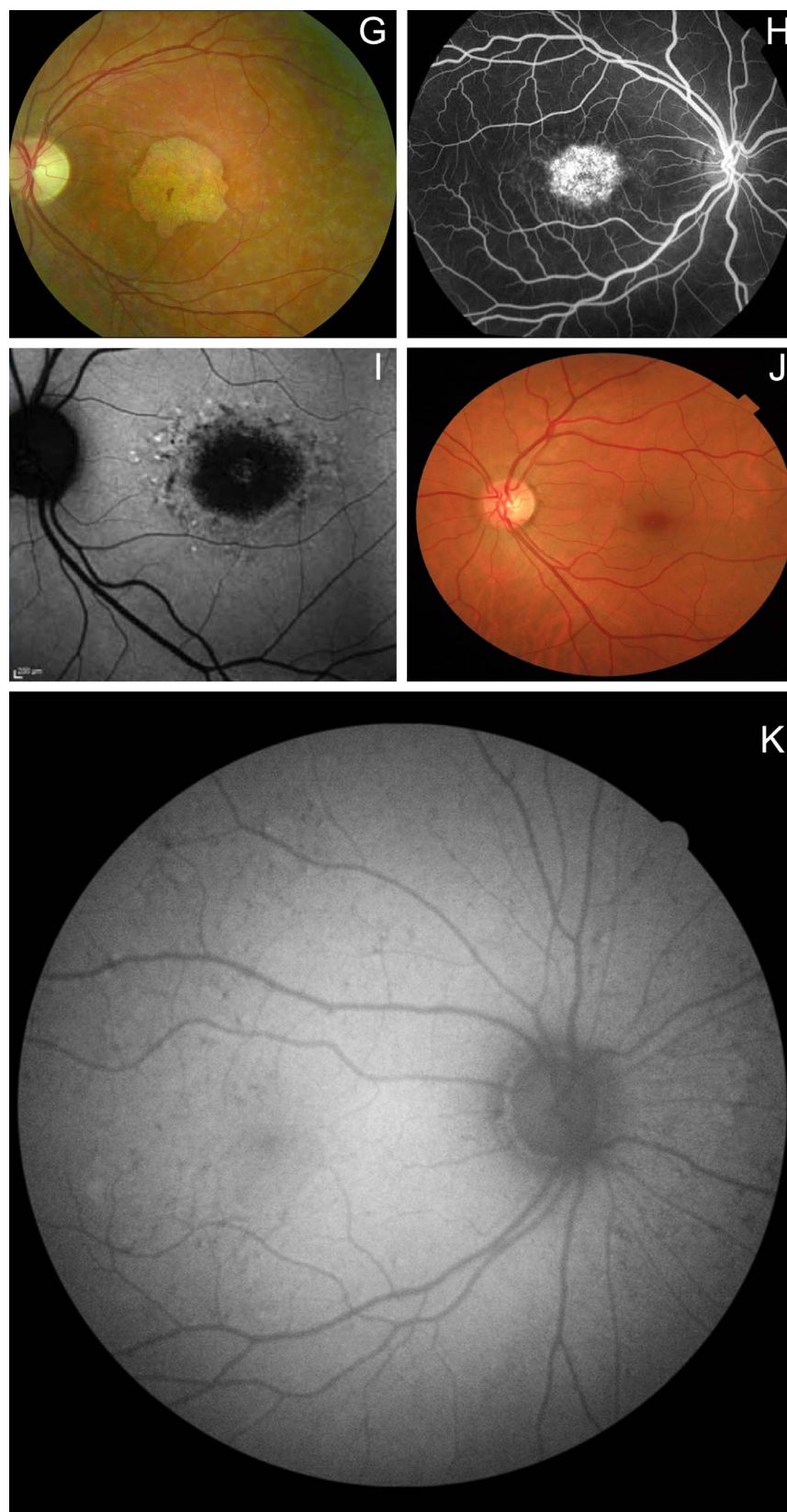


FIGURE 1. Continued.

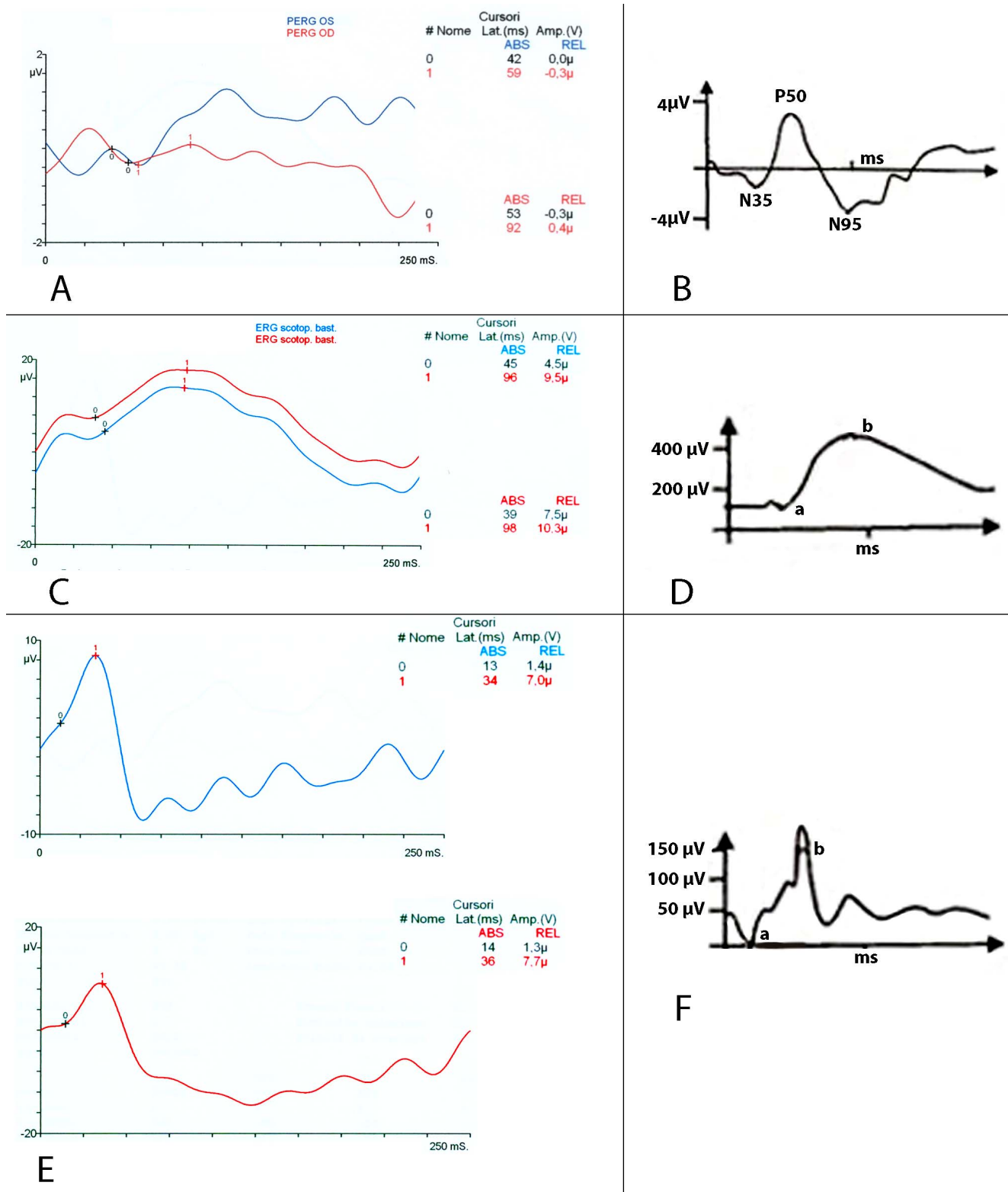


FIGURE 2. Proband's ERG and PERG, compared with healthy control. PERG (A) The voltage of the P50 wave was abnormally decreased and the latency was increased. The scotopic (C) and photopic (E) ERGs showed abnormally low voltage. The combination of this data suggests an impairment of both rods and cones functions, compared with PERG (B), scotopic (D), and photopic (F) reference ERGs. The signal was amplified (gain 50,000), filtered (band pass, 1–100 Hz) and averaged with automatic rejection of artifacts by a BM 6000 unit. Analysis time was 250 msec. In healthy subjects, these peaks have the following implicit times: 35, 50, and 95 msec (N35, P50, N95).

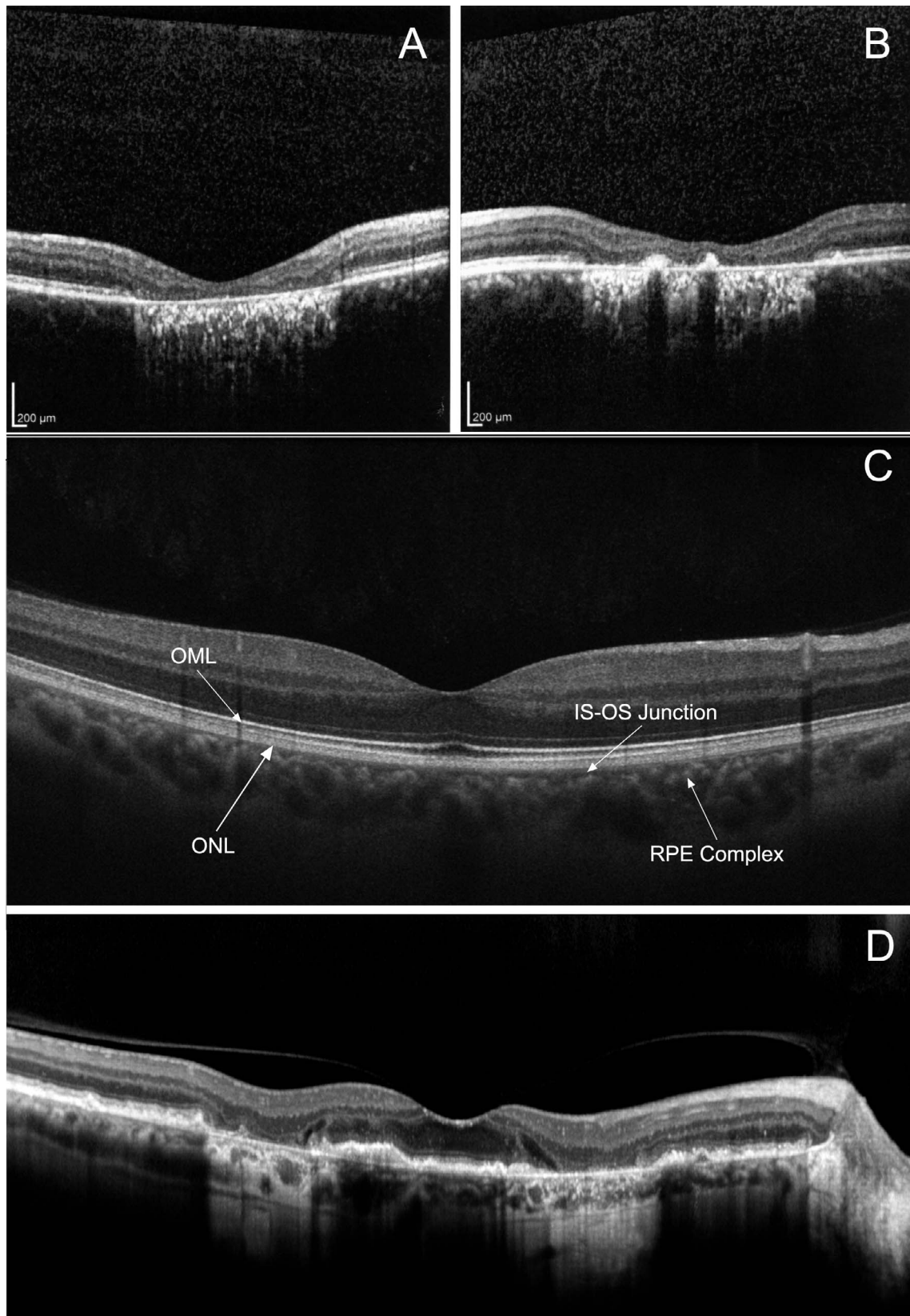


FIGURE 3. OCT of proband (A, B), compared with that of a healthy control (C) and overt STDG3 patient (D). Proband's right eye (A) depicts the extent of the transverse loss of the junction between the inner and outer segment of the photoreceptors in the foveal region. Furthermore, his left eye (B) showed abnormal pigmentation in the RPE layer, due to macular degeneration, as notable in the STDG3 patient (D). The integrity of all retina layers in a healthy subject is highlighted in (C).

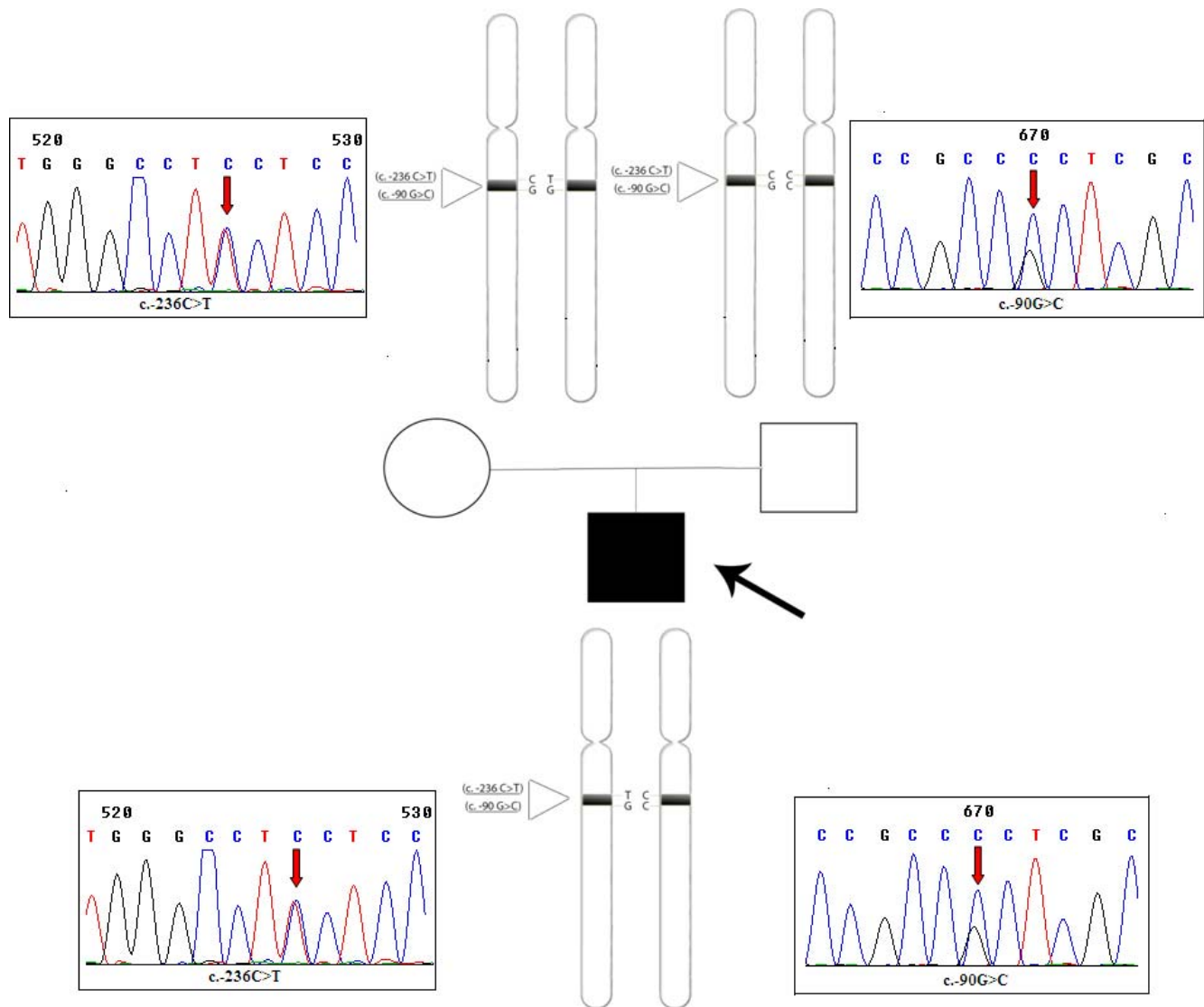


FIGURE 4. Family tree genotypes and sequencing peaks for *ELOVL4* (6q14.1). Mutated condition, due to present polymorphisms, is *underlined*. Black arrow indicates the proband.

Novel constructs were subcloned into *Escherichia coli* Top 10 cells (Life Technologies) and single colonies were miniprep. The correct sequence of all the clones was verified by DNA sequencing, using the Sanger method, and then selected for transient transfection.

Transient Transfection and Promoter Assays

Cells were first seeded in 96-well culture plates at a density of 2×10^4 cells per well. Then, a transient transfection was performed with following modality: (1) in 1/4 of wells (16), cells were cotransfected with 0.05 μ g of the pGL4.10 [*luc2*] promoter construct containing the only c.-90 G>C variant, and with 0.05 μ g of the pGL4.10 [*luc2*] promoter construct containing the *ELOVL4* wild-type promoter; (2) in a second 1/4 of wells (16), cells were cotransfected with 0.1 μ g of the pGL4.10 [*luc2*] promoter construct containing only the c.-236 C>T variant, and with 0.05 μ g of the pGL4.10 [*luc2*] promoter construct containing the *ELOVL4* wild-type promoter; (3) in another 1/4 of wells (16), cells were cotransfected with 0.05 μ g of two pGL4.10 [*luc2*] promoter constructs containing, respectively, the c.-90 G>C and the c.-236 C>T variants; and

(4) in the final quarter of wells (16), cells were transfected with 0.1 μ g of the pGL4.10 [*luc2*] promoter construct containing the *ELOVL4* wild-type promoter. Finally, the remaining 32 wells were filled with not transfected cells (16) and with the luciferase substrate only (16). In each well, besides cells, the mixture included 0.2 μ L of Lipofectamine 3000 Reagent (ThermoFisher Scientific, Waltham, MA, USA) and 0.2 μ L of P3000 Reagent (ThermoFisher Scientific), in a serum-free medium and then incubated for 24 hours at 37°C in a humidified atmosphere of 5% CO₂ in air. After incubation, cells were washed twice with PBS and lysed by Passive Lysis Buffer (Promega). Luciferase activity was measured using Dual-Luciferase assay kit (Promega) and GloMax-Luminometer (Promega). Reporter construct activity was normalized by comparison with activity from the *Renilla* luciferase construct. Luciferase activities are representative of at least six independent experiments, with each construct tested 16 times per experiment.

Population Screening

Analyzed variants were screened in 500 unrelated healthy donors born and living in Messina for at least two generations,

constituting a heterogeneous group for age and sex, in order to assess their frequency in the same geographic site population in which the patients belonged.

Statistical Analysis

All data analyses were performed using the IBM SPSS 24 software for Macintosh (IBM SPSS Statistics for Macintosh; IBM Corp, Armonk, NY, USA). A 1-way ANOVA was performed to compare between the sample groups. All *P* values were Bonferroni's corrected and considered significant if *P* < 0.05.

Ethical Statements

The study followed the tenets of the Declaration of Helsinki and was approved by the Scientific Ethics Committee of the Azienda Ospedaliera Universitaria-Policlinico "G. Martini" Messina. All family members and controls signed informed consent after explanation of the nature and possible consequences of the study.

RESULTS

Genotyping of *ELOVL4* promoter in the whole family components highlighted that the proband's mother and father present an alternate heterozygosity for each variant in exam (Fig. 4), indicating that the proband inherited both variants in trans. The predictive analysis of the proband's *ELOVL4* promoter by TRANSFAC Professional evidenced the loss of one group of TF binding sites (ETF, ZF5, E2F-6, FBI-I, HDAC2, and TAFII250) in the double heterozygous genotype, due to the presence of c.-90 G>C for most of them. The exception was represented by FBI-I and the complement 666 through 679 binding sites for TAFII250, whose loss was attributable to c.-236 C>T. A second group analysis, resulting from the combined predictions of TRANSFAC and PROMO, revealed the appearance of new possible binding sites of different TFs (CPB, BCL6B secondary motif, Spi-B, Pax-4, RXR-alpha, GKLF, POLR3A, TFII-I, Pax-5, p53, SP1, and GR-alpha), determined by c.-236 C>T for Spi-B, Pax-4 and RXR-alpha, and by c.-90 G>C for others (for further details see Table 1). This data suggest a probable transcription variation, due to the altered balance of TF binding properties. Furthermore, it is important to understand the relationship between the analyzed TFs, and how each one could influence the others. This was examined by Cytoscape pathway analysis, along with its MCODE plug-in, from which arose a 4-cluster division that highlighted a relevant network involving most of the TFs in exam (Table 2; Fig. 5). These data were confirmed by Dual-Luciferase Reporter Assay, involving the proband's *ELOVL4* promoter, compared in its wild form, versus both variants and c.-90 G>C and c.-236 C>T only samples. Results showed an expression reduction of approximately 14% in the c.-90 G>C sample and of approximately 18% in the c.-236 C>T one (compared with a healthy control), but a strong decrease (~97%) arose from the promoter carrying the combination of above variants (Fig. 6). The 1-way ANOVA, after Bonferroni's correction, confirmed the statistical significance of analysis (*P* < 0.05). Multiple comparison details are listed in Supplementary Materials.

These results take a particular value, considering that both analyzed variants showed a very low frequency distribution in Messina healthy population (c.-90 G>C: G frequency = 0.94, C frequency = 0.06; c. 236 C>T: C frequency = 0.95%, T frequency = 0.05), in contrast to what reported in the European population (in the public domain, http://www.ensembl.org/Homo_sapiens/Variation/Population?db=core;r=6:79946869-79947869;v=rs62407622;vdb=variation;vf=12792

675; in the public domain, http://www.ensembl.org/Homo_sapiens/Variation/Population?db=core;r=6:79947015-79948015;v=rs240307;vdb=variation;vf=129670).

DISCUSSION

ELOVL4 encodes a member of the elongase family, expressed in retina, brain, skin, and sperm, involved in the elongation of very long-chain fatty acids.¹⁰ Although little is known about the role of this protein, data report that the contribution of the enzyme is to be found in the initial rate of VLC-PUFA production and condensation reactions between a fatty acyl-CoA and malonyl-CoA.⁵ The role of VLC-PUFA is fundamental. The most reliable hypothesis argues that the VLC-PUFA acyl chain may cover the entire bilayer, representing a flexible hinge at the rim site where the curvature of photoreceptor disk membranes is the greatest.⁹ At rim level, alteration of *ELOVL4* could impair the turnover of photoreceptor disk membranes, due to a modified balance of fatty acid precursors. The direct consequence of this variation leads to an abnormal accumulation of lipofuscin granules, observed in the RPE of mutant retinas that may impair retinoic acid trafficking between RPE and photoreceptors.²³

Recent experiments have shown a reduction in rods ERG oscillatory potentials and scotopic threshold responses in *ELOVL4* KO mice, and presented biomorphologic evidence that the ERG changes are correlated with reduced VLC-PUFA and synaptic architecture. It may affect vesicle tethering or recycling pathways, as well as glutamate release mechanisms, due to VLC-PUFA interaction with synaptic proteins that mediate endo/exocytic activity or that were localized to the synaptic ribbon in photoreceptor terminals.¹³

It is known that *ELOVL4* mutations, alone or with *PROM1* mutations, could cause enzyme activity loss and, subsequently, the onset of the dominant form of STGD.²⁴

Analysis of *ELOVL4* gene sequence in our patient affected by STGD permitted us to identify two variants, transconfigured on the gene promoter. We demonstrated that the coexistence of two variants determined the down regulation of gene transcription. To be precise, the Dual-Luciferase Reporter assay highlighted the down regulation of *ELOVL4* transcription by 97% in the patient's sample (c.-90 G>C and c.-236 C>T). The possible protein elongating activity loss could lead to several consequences:

1. Compromising the integrity of photoreceptor membrane compartments, such as Golgi, or even the retinal pigment epithelium²⁵;
2. Causing a corresponding reduction of rhodopsin levels within outer segment disk membranes, or the production of abnormal hetero-oligomers with its membrane proteins, which may lead to alterations in membrane ultrastructure or biochemistry²⁶; and
3. Altering VLC-PUFA direct signaling and possible alteration of the rim site where the curvature of photoreceptor disk membranes is greater or the greatest. It was proposed that lipid molecules, such as docosahexaenoic (DHA), eicosapentaenoic, and arachidonic acids could activate specific receptors or modulate transient receptor potential cation channel activity. The latter task is enforced by the presence of VLC-PUFAs also in ribbon synapses, as well as the smaller conventional synapses in the retina.¹³

Results showed that many TF binding sites were altered in the *ELOVL4* promoter, both for activators (ETF,²⁷ FBI-I,²⁸ HDAC2,²⁹⁻³² and TAFII250,^{33,34} Spi-B,³⁵ Pax-4,^{36,37} POLR3A,^{38,39} TFII-I,^{40,41} PAX-5,^{42,43} TP53,⁴⁴⁻⁴⁶ SP1,⁴⁷⁻⁴⁹ and GR-

TABLE 1. BioBase and TRANSFAC TFs Binding Sites Prediction

BioBaseTransfac										
Factor Name	Region	Strand	Match Sequence	Core Similarity	Matrix Similarity	Matrix ID	WT	c.-236 C>T c.-90 G>C	c.-236 C>T c.-90 G>C	Reference (PMID)
ETF	807..813	minus	CGGCCgc	1	1	V\$ETF_Q6	✓	✓	✓	2768275
ZF5	810..817	minus	cgcCTGC	0.844	0.896	V\$ZF5_Q1	✓	✓	✓	17714511
EZF-6	811..819	minus	cgcTCGCC	0.69	0.787	V\$EZF6_Q2	✓	✓	✓	9501179
FBF1	660..668	minus	gGGCTctt	0.625	0.79	V\$ZBTB7A_Q2	✓	✓	✓	19853566; 15917220
HDAC2	811..819	plus	CGCTGccc	0.829	0.82	V\$HDAC2_Q4	✓	✓	✓	26129908; 23940731; 23696608
TAFII250	666..679	minus	CCTCCacctctcg	0.807	0.84	V\$TAF1_Q5	✓	✓	✓	18171927
	804..812	plus	cGGCCGccg	0.795	0.846	V\$TAF1_Q6	✓	✓	✓	
	804..812	minus	cggCCGccg	0.798	0.849	V\$TAF1_Q6	✓	✓	✓	
	806..814	plus	GCCGCcgct	1	0.984	V\$TAF1_Q7	✓	✓	✓	
CPBP	809..815	plus	GCCCCtc	1	1	V\$CPBP_Q6	✓	✓	✓	24906860; 17893646; 16431954
BCL6B	803..818	plus	ccggcGGCCctcgcc	1	0.979	V\$BCL6B_Q4	✓	✓	✓	23057762
Sp1B	665..670	plus	TTCTCc	1	1	V\$SP1B_Q3	✓	✓	✓	1406622
Pax-4	664..674	plus	ctctCCACct	1	0.918	V\$PAX4_Q2	✓	✓	✓	19843539; 19012751
RXRalpha	662..668	minus	gcCTTCT	0.972	0.982	V\$RXRA_Q10	✓	✓	✓	26310807; 19427305; 10520230
GKLF	810..822	minus	cCCCTCgcccctg	0.989	0.989	V\$GKLF_Q3_Q1	✓	✓	✓	27022622
POLR3A	812..824	minus	cctCGCCcctg	0.944	0.962	V\$POLR3A_Q1	✓	✓	✓	19176527; 9331371

Allgene PROMO										
Factor Name	Region	Strand	Match Sequence	Dissimilarity	RE Equally	RE Query	WT	c.-236 C>T c.-90 G>C	c.-236 C>T c.-90 G>C	Reference (PMID)
TFIIH	664..669	plus	TTCTCC	11.337888	1.24512	1.92792	✓	✓	✓	17239664
PAX-5	805..811	plus	GCCGCC	9.552105	0.74707	1.9483	✓	✓	✓	22278416
TP53	805..811	plus	GCCGCC	6.188498	0.31128	0.91106	✓	✓	✓	26439195; 25407019
SP1	803..812	plus	cGGCCGCC	3.170707	0.01751	0.09628	✓	✓	✓	26078979; 25552121
GR-alpha	811..815	plus	CCTCG	8.281568	3.98438	5.91804	✓	✓	✓	23211818

Factor name, binding factor name, represented by the matrix; Region, position of the matrix match (putative binding site) within the analyzed sequence; Strand (plus/minus), the strand on which the putative site was found depends on the orientation in which the matrix is given in TRANSFAC; Match sequence, capital letters indicate the positions in the sequence that match with the core sequence of the matrix, while the lower case letters refer to positions that match to the remaining part of the matrix; Core similarity, the core similarity score for the matrix match (the matrix core is defined as the five consecutive most conserved nucleotides within the matrix); Matrix similarity, the matrix similarity score for the matrix match. The Match score can vary from 0 (lowest similarity) to 1 (highest similarity) of the match to the matrix. Only those matches are listed in the result, for which the core and matrix similarity are higher than the chosen cutoffs; Matrix ID, identifier for the matrix with which the putative binding site was found; Dissimilarity, the dissimilarity threshold controls how similar a sequence must be to the matrix to be reported as a hit. It was set at 15% (85% similarity). Random expectation (RE), gives the number of expected occurrences of the match in a random sequence of the same length as the query sequence according to the dissimilarity index. Two models are considered: (1) Equiprobability for the 4 nucleotides (RE equally), and (2) Estimate the nucleotide probabilities as the nucleotide frequencies in the query sequence (RE query).

Results from these two software analyses highlight the appearance or disappearance of specific TFs binding sites in the presence of no analyzed mutations (wild-type column), both examined ones (c.-236 C>T, c.-90 G>C column), and single separated variants (respectively, c.-90 G>C column, and c.-236 C>T column).

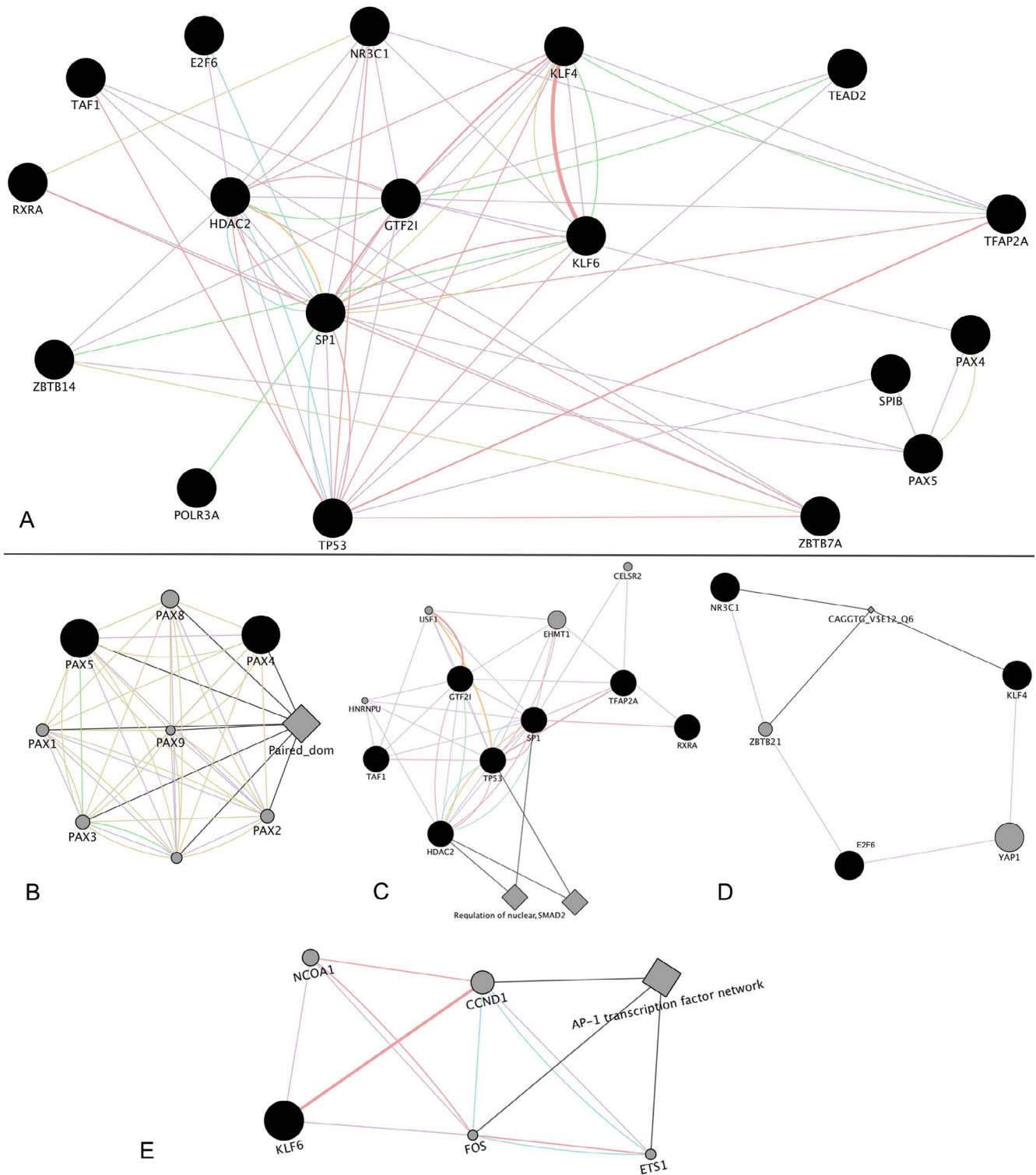


FIGURE 5. Cytoscape images from network views. This shows the Cytoscape pathways analysis, supported by GeneMANIA and MCODE plug-ins, with nodes and edges reflecting relationships between query TFs involved in *ELOVL4* expression. Edge colors: Coexpression (light purple), physical interaction (antique pink), genetic interaction (green), shared protein domains (golden yellow), pathway (light blue), predicted (orange), and common function (gray). (A) Graphic representation of all TFs in exam relationship. (B–E). MCODE clustering analysis, which evidences that most of the query TFs could be grouped into four functional and/or structural clusters.

alpha^{50,51}) and repressors (ZF5,⁵² EZF-6,⁵³ CPBP,^{54–56} BCL6B,⁵⁷ GKLF,^{58–60} and RXR-alpha^{61–64}).

We can speculate that, as emerges from Cytoscape pathway analysis, the *ELOVL4* expression reduction in the proband

could derive from a complex balance of all TFs, most of which could present a mutual influence in determining the final effect. Focusing on TFs binding sites formed as a result of the presence of both examined variants, SP1 probably represents

Investigative Ophthalmology & Visual Science

TABLE 2. Cytoscape Pathway Analysis of TFs Involved Into ELOVL4 Promoter Integrity

Gene Name	Annotations (GO ID)	Ensembl Protein ID	Entrez Gene ID	RefSeq mRNA ID	UniProt ID	Score	Log Score	MCODE Node_Status	MCODE_Cluster	MCODE_Score
<i>KLF4</i>	GO:0048598 GO:0001159 GO:0000976 GO:0000790 GO:0019827 GO:0044212 GO:0000981 GO:0000975 GO:0000785 GO:0043565 GO:0001085 GO:0044454 GO:0000987 GO:0000228 GO:0001228	ENSP00000040922	9314	NM_004235	O43474	0.653	-0.426	Clustered	Cluster 4	3.692
<i>KLF6</i>	GO:0003690 GO:0003700 GO:0005515 GO:0046872	ENSP000000445301	1316	NM_001300	Q99612	0.670	-0.400	Clustered	Cluster 3	5.333
<i>E2F6</i>	GO:0003677 GO:0003700 GO:0003714 GO:0005515	ENSP000000446315	1876	NM_212540	O75461	0.605	-0.502	Seed	Cluster 4	3.733
<i>GTF2I</i>	GO:0006367 GO:0006352	ENSP000000460070	2969	NM_033001	P78347	0.562	-0.577	Clustered	Cluster 2	4.200
<i>TAF1</i>	GO:0006367 GO:0000975 GO:0003713 GO:0043565 GO:0006352 GO:0016570 GO:0044212 GO:0002039 GO:0001067	ENSP000000424526	6872	NM_138923	TAF1_HUMAN	0.719	-0.330	Clustered	Cluster 2	4.167
<i>RXR4</i>	GO:0000981 GO:0006367 GO:0000975 GO:0000785 GO:0003713 GO:0000790 GO:0006352 GO:0044454 GO:0000228 GO:0044212 GO:0001067	ENSP000000470812	6256	NM_002957	RXRA_HUMAN	0.616	-0.484	Clustered	Cluster 2	4.000
<i>ZBTB7A</i>	GO:0000978 GO:0001078 GO:0003677 GO:0003700 GO:0005515	ENSP000000471865	51341	NM_015898	ZBT7A_HUMAN	0.770	-0.262	Unclustered	/	2.311
<i>HDAC2</i>	GO:0048598 GO:0000785 GO:0043565 GO:0001085 GO:0000790 GO:0044454 GO:0000228 GO:0016570	ENSP000000430432	3066	NM_001527	Q92769	0.588	-0.531	Clustered	Cluster 2	3.889
<i>PAX5</i>	GO:0000978 GO:0001077 GO:0003677 GO:0003700 GO:0005515	ENSP000000431038	5079	NM_016734	Q02548	0.702	-0.354	Clustered	Cluster 1	8.000
<i>NR3C1</i>	GO:0006367 GO:0006352	ENSP000000427672	2908	NM_001204264	P04150	0.583	-0.539	Clustered	Cluster 4	3.714
<i>SP1B</i>	GO:0003700 GO:0043565	ENSP000000472626	6689	NM_003121	SP1B_HUMAN	0.644	-0.440	Unclustered	Clustered	2.700
<i>TP53</i>	GO:0000790 GO:0000377 GO:0044212 GO:0002039 GO:0000981 GO:0000975 GO:0000785 GO:0001085 GO:0044454 GO:0000228 GO:0001228 GO:0016570 GO:0001067	ENSP000000473895	7157	NM_001276761	P53_HUMAN	0.547	-0.603	Clustered	Cluster 2	4.209
<i>SP1</i>	GO:0006367 GO:0001159 GO:0000975 GO:0000976 GO:0043565 GO:0001085 GO:0006352 GO:0000987 GO:0042826 GO:0044212 GO:0001067	ENSP000000458133	6667	NM_138473	SP1_HUMAN	0.586	-0.534	Seed	Cluster 2	4.678
<i>PAX4</i>	GO:0000980 GO:0001206 GO:0003677 GO:0003690 GO:0005515	ENSP000000473846	5078	NM_006193	PAX4_HUMAN	0.769	-0.262	Clustered	Cluster 1	8.000
<i>ZBTB14</i>	GO:0000977 GO:0000981 GO:0003700 GO:0005515 GO:0043565	ENSP000000463555	7541	NM_003409	ZBT14_HUMAN	0.730	-0.315	Unclustered	/	3.467
<i>TFAP2A</i>	GO:0048598 GO:0001159 GO:0000976 GO:0016331 GO:0042472 GO:0048839 GO:2000377 GO:0044212 GO:0000981 GO:0000975 GO:0003713 GO:0043583 GO:0043565 GO:0000987 GO:0001228 GO:0042471 GO:0001067	ENSP000000420568	7020	NM_003220	P05549	0.725	-0.321	Clustered	Cluster 2	4.182
<i>POLR34</i>	GO:0001056 GO:0003677 GO:0003682 GO:0003899 GO:0008270	ENSP000000473389	11128	NM_007055	RPC1_HUMAN	0.807	-0.214	Unclustered	/	2.000
<i>TEAD2</i>	GO:0006367 GO:0006352	ENSP000000472397	8463	NM_003598	TEAD2_HUMAN	0.817	-0.203	Unclustered	/	1.533

Gene name, name of the gene that encodes for one of involved transcription factor. Annotation (GO ID), ID associated to gene ontology. The GO classifies gene functions along three aspects: (1) molecular function, (2) cellular component, and (3) biological process; Ensembl protein ID, protein ID for Ensembl; Entrez gene ID, gene ID for Entrez; RefSeq mRNA ID, mRNA ID for NCBI Reference Sequence Database; UniProt ID, UniProt protein ID score. Prior to construction, the selected networks are each assigned a weight by the GeneMANIA algorithm. The query genes are assigned a label value of 1, while all other genes are 0. Label propagation is then applied to the entire network and the resulting labels are saved as the score attribute, used to rank the genes. The score assigned to each gene reflects how often paths starting at a given gene node end up in one of the query nodes and how long and heavily weighted those paths are. This score indicates the relevance of each gene to the original list based on the selected networks. Higher scores indicate genes that are more likely to be functionally related. We also chose not to add any other genes coming from pathway analysis to visualize only how the members of our list are connected; Log score, logarithmic scale applied to score values; MCODE cluster, indicates the number of cluster analyzed genes belong to; MCODE Node Status, no evidence if query gene is part of a cluster; MCODE Score represents the highest scoring node in the cluster; MCODE Status defines the weight value that permit a gene to be clustered; Unclustered genes typically show the lowest value.

Pathways analysis by Cytoscape and its plugins GeneMANIA and MCODE revealed a strict interaction between all TFs whose binding sites presence/absence is determined by examined variants.

SAMPLE	<u>c. -90 G>C</u>	<u>C. -236 C>T</u>	<u>c. -236 C>T</u> <u>c. -90 G>C</u>	Control	Not Transf. Cells.	Substrate only
MEAN	2,262	2,040	0,810	2,502	0,773	0,772
SD	0,045	0,040	0,063	0,049	0,046	0,010
SEM	0,011	0,010	0,016	0,012	0,011	0,002

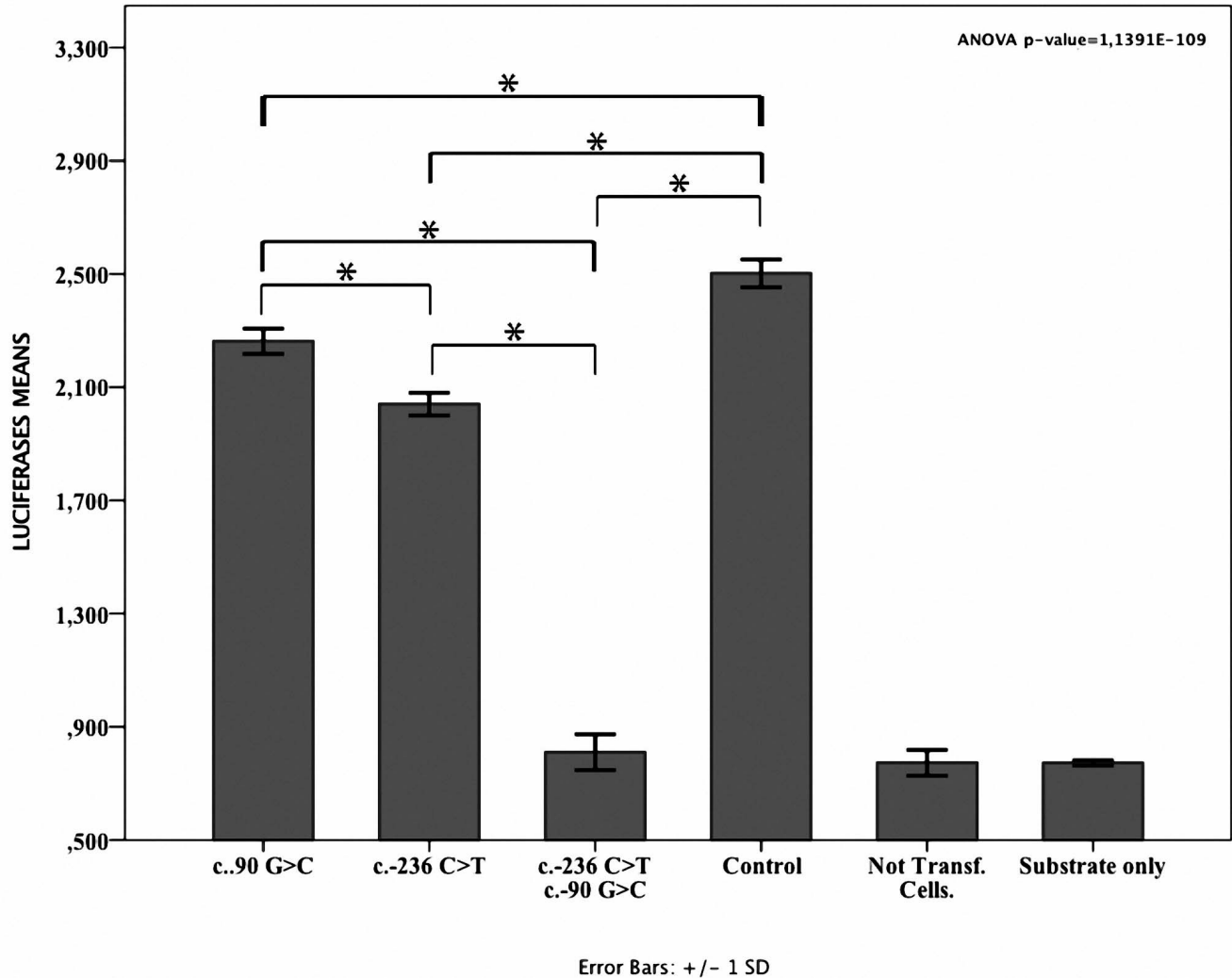


FIGURE 6. Luciferase assay results. The histogram shows the means coming from luciferase ratios between Firefly and Renilla bioluminescence measurements (in relative luminescence units - LRU) for each sample. As reported, ANOVA test resulted significant ($P = 1.1391 \times 10^{-109}$), also for multiple comparisons (highlighted with pairwise lines on bars and asterisk). The presence of only the c.-90 G>C or the c. 236 C>T variant determines an *ELOVL4* expression reduction, respectively, of approximately 14% or 18%, compared with the healthy control, while the heterozygous condition for both examined variants drastically lowers it (~97%).

the key node around which other factors determine the overall *ELOVL4* protein under expression. As literature evidences, SP1 should be enhanced by RXR-alpha activity,⁶⁵ but this positive status should be repressed or seized by interaction with TFII-I,⁶⁶ TP53,⁶⁷ and KLF6,⁶⁸ the latter stimulated by KLF4.⁶⁹ The direct consequences of SP1 inhibition could be related to a decrease of connected PAX-5,^{70,71} in turn influencing PAX-4.⁷² Although there is no solid proof, in literature, of a possible direct interaction, we can hypothesize, basing on previous assumptions, that TFII-I, usually acting as a repressor, could contribute to the inhibition of SP1, as well as the possibility that SP1 impairment could reflect on POLR3A, reducing its activity.

Due to the unavailability of data on involved TF interactions, analysis on TF binding sites lost in the patient is not clear. We can only speculate that, because HDAC2 usually acts as a repressor, with FBI as corepressor,⁷³ both could downregulate another two inhibitors, ZF5 and E2F-6. This situation leaves most of the transcriptional activity to TAFII250, which functions as an activator, and which presents many binding sites in wild-type genotype.

CONCLUSIONS

A reduction of *Elovl4* enzymatic function in the endoplasmic reticulum (ER) could result in a deficiency of VLC-PUFA,

which may be required for the construction, function, and maintenance of healthy OS or other photoreceptor membranes; hence, the absence of sufficient quantities eventually results in retinal degeneration. The results presented here reported reduced ELOVL4 enzyme activity, fundamental in VLC-PUFA synthesis, vital for rod function and rod longevity, parameters that are involved in the etiopathogenesis of STGD.

We speculate that an altered balance of TF binding sites, due to the presence of c.-90 G>C and c.-236 C>T, and the possible interaction of involved transcription factors, could determine an overall prevalence of repressive activity rather than enhancing activity, resulting in a downregulation of ELOVL4 expression, as functionally demonstrated by the dual-luciferase reporter assay.

Even if the in vitro experiments demonstrate an expression reduction of ELOVL4 promoter due to transconfiguration of analyzed variants, we cannot assert with certainty that the same effect, in vivo, is limited to both variants' presence. For example, cells are treated outside their normal 'microenvironment' (no surrounding tissues, no blood supply, no normal supply of nutrients, etc.), and we cannot exclude the involvement of other factors into the altered expression of ELOVL4. Moreover, further experiments (e.g., ChIP-Sequencing of involved TFs) will be needed to confirm, or not, the role of single transcription factors and reciprocal interactions, involved in ELOVL4 downregulation.

Acknowledgments

The authors thank all of the study participants.

Disclosure: **L. Donato**, None; **C. Scimone**, None; **C. Rinaldi**, None; **P. Aragona**, None; **S. Briuglia**, None; **A. D'Ascola**, None; **R. D'Angelo**, None; **A. Sidoti**, None

References

- Jiang, F, Pan, Z, Xu K, et al. Screening of ABCA4 gene in a chinese cohort with Stargardt disease or cone-rod dystrophy with a report on 85 novel mutations. *Invest Ophthalmol Vis Sci.* 2016;57:145-152.
- Lansel N, Niemeyer G, Thölen A. Stargardt's disease and its intrafamilial variability [in German]. *Klin Monbl Augenbeilkd.* 2000;216:342-345.
- Tanna P, Strauss RW, Fujinami K, Michaelides M. Stargardt disease: clinical features, molecular genetics, animal models and therapeutic options. *Br J Ophthalmol.* 2017;101:25-30.
- Yi J, Li S, Jia X, et al. Evaluation of the ELOVL4, PRPH2 and ABCA4 genes in patients with Stargardt macular degeneration. *Mol Med Rep.* 2012;6:1045-1049.
- Agbaga MP, Tam BM, Wong JS, Yang LL, Anderson RE, Moritz OL. Mutant ELOVL4 that causes autosomal dominant Stargardt-3 macular dystrophy is misrouted to rod outer segment disks. *Invest Ophthalmol Vis Sci.* 2014;55:3669-3680.
- Logan S, Anderson RE. Dominant Stargardt macular dystrophy (STGD3) and ELOVL4. *Adv Exp Med Biol.* 2014;801:447-453.
- Bardak H, Gunay M, Erçalık Y, et al. Analysis of ELOVL4 and PRPH2 genes in Turkish Stargardt disease patients. *Genet Mol Res.* 2016;15:gmr15048774.
- Tran HV, Moret E, Vaclavik V, et al. Swiss family with dominant Stargardt disease caused by a recurrent mutation in the ELOVL4 gene. *Klin Monbl Augenbeilkd.* 2016;233:475-477.
- Harkewicz R, Du H, Tong Z, et al. Essential role of elovl4 protein in very long chain fatty acid synthesis and retinal function. *J Biol Chem.* 2012;287:11469-11480.
- Bennett LD, Anderson RE. Current progress in deciphering importance of VLC-PUFA in the retina. *Adv Exp Med Biol.* 2016;854:145-151.
- Marchette LD, Sherry DM, Brush RS, et al. Very long chain polyunsaturated fatty acids and rod cell structure and function. *Adv Exp Med Biol.* 2014;801:637-645.
- Logan S, Agbaga MP, Chan MD, et al. Deciphering mutant ELOVL4 activity in autosomal-dominant Stargardt macular dystrophy. *Proc Natl Acad Sci U S A.* 2013;110:5446-5451.
- Bennett LD, Hopiavuori BR, Brush RS, et al. Examination of VLC-PUFA-deficient photoreceptor terminals. *Invest Ophthalmol Vis Sci.* 2014;55:4063-4072.
- Ayyagari R, Zhang K, Hutchinson A, et al. Evaluation of the ELOVL4 gene in patients with age-related macular degeneration. *Ophthalmic Genet.* 2001;22:233-239.
- Aguilà M, Bevilacqua D, McCulley C, et al. Hsp90 inhibition protects against inherited retinal degeneration. *Hum Mol Genet.* 2014;23:2164-2175.
- Matys V, Kel-Margoulis OV, Fricke E, et al. TRANSFAC and its module TRANScmpel: transcriptional gene regulation in eukaryotes. *Nucleic Acids Res.* 2006;34:D108-D110.
- Farré D, Roset R, Huerta M, et al. Identification of patterns in biological sequences at the ALGGEN server: PROMO and MALGEN. *Nucleic Acids Res.* 2003;31:3651-3653.
- Scimone C, Bramanti P, Ruggeri A, et al. CCM3/SERPINI1 bidirectional promoter variants in patients with cerebral cavernous malformations: a molecular and functional study. *BMC Med Genet.* 2016;17:74.
- Tzeng DT, Tseng YT, Ung M, Liao IE, Liu CC, Cheng C. DPRP: a database of phenotype-specific regulatory programs derived from transcription factor binding data. *Nucleic Acids Res.* 2014;42:D178-D183.
- Liu X, Yu X, Zack DJ, Zhu H, Qian J. TiGER: a database for tissue-specific gene expression and regulation. *BMC Bioinformatics.* 2008;9:271.
- Rheinbay E, Suvà ML, Gillespie SM, et al. An aberrant transcription factor network essential for Wnt signaling and stem cell maintenance in glioblastoma. *Cell Rep.* 2013;3:1567-1579.
- Myšičková A, Vingron M. Detection of interacting transcription factors in human tissues using predicted DNA binding affinity. *BMC Genomics.* 2012;13(suppl 1):S2.
- Bennett LD, Brush RS, Chan M, et al. Effect of reduced retinal VLC-PUFA on rod and cone photoreceptors. *Invest Ophthalmol Vis Sci.* 2014;55:3150-3157.
- Palejwala NV, Gale MJ, Clark RF, Schlechter C, Weleber RG, Pennesi ME. Insights into autosomal dominant Stargardt-like macular dystrophy through multimodality diagnostic imaging. *Retina.* 2016;36:119-130.
- Vasireddy V, Jablonski MM, Khan NW, et al. ELOVL4 5-bp deletion knock-in mouse model for Stargardt-like macular degeneration demonstrates accumulation of elovl4 and lipofuscin. *Exp Eye Res.* 2009;89:905-912.
- Okuda A, Naganuma T, Ohno Y, et al. Hetero-oligomeric interactions of an elovl4 mutant protein: implications in the molecular mechanism of Stargardt-3 macular dystrophy. *Mol Vis.* 2010;16:438-445.
- Kageyama R, Merlino GT, Pastan I. Nuclear factor ETF specifically stimulates transcription from promoters without a TATA box. *J Biol Chem.* 1989;264:15508-15514.
- Maeda T, Ito K, Merghoub T, et al. LRF is an essential downstream target of GATA1 in erythroid development and regulates BIM-dependent apoptosis. *Dev Cell.* 2009;17:527-540.

29. Fan J, Alsarraf O, Dahrouj M, et al. Inhibition of HDAC2 protects the retina from ischemic injury. *Invest Ophthalmol Vis Sci.* 2013;54:4072-4080.
30. Kong X, Fang M, Li P, Fang F, Xu Y. HDAC2 deacetylates class II transactivator and suppresses its activity in macrophages and smooth muscle cells. *J Mol Cell Cardiol.* 2009;46:292-299.
31. Koriyama Y, Takagi Y, Chiba, K, et al. Requirement of retinoic acid receptor β for genipin derivative-induced optic nerve regeneration in adult rat retina. *PLoS One.* 2013;8:e71252.
32. Lebrun-Julien F, Suter U. Combined HDAC1 and HDAC2 depletion promotes retinal ganglion cell survival after injury through reduction of p53 target gene expression. *ASN Neuro.* 2015;7:pii:1759091415593066.
33. Herzfeld T, Nolte D, Müller U. Structural and functional analysis of the human TAF1/DYT3 multiple transcript system. *Mamm Genome.* 2007;18:787-795.
34. Piper M, Dwivwdy A, Leung L, Bradley RS, Holt CE. NF-protocadherin and TAF1 regulate retinal axon initiation and elongation in vivo. *J Neurosci.* 2008;28:100-105.
35. Ray D, Bosselut R, Ghysdael J, Mattei MG, Tavitian A, Moreau-Gachelin F. Characterization of Spi-B, a transcription factor related to the putative oncoprotein Spi-1/PU.1. *Mol Cell Biol.* 1992;12:4297-4304.
36. Rath ME, Bailey MJ, Kim JS, Coon SL, Klein DC, Møller M. Developmental and daily expression of the PAX4 and PAX6 homeobox genes in the rat retina: localization of PAX4 in photoreceptor cells. *J Neurochem.* 2009;108:285-294.
37. Reichman S, Kalathur RK, Lambard S, et al. The homeobox gene CHX10/VSX2 regulates RDCVF promoter activity in the inner retina. *Hum Mol Genet.* 2010;19:250-261.
38. Natalizio BJ, Robson-Dixon ND, Garcia-Blanco MA. The carboxyl-terminal domain of RNA polymerase II is not sufficient to enhance the efficiency of pre-mRNA capping or splicing in the context of a different polymerase. *J Biol Chem.* 2009;284:8692-8702.
39. Sepehri S, Hernandez N. The largest subunit of human RNA polymerase III is closely related to the largest subunit of yeast and trypanosome RNA polymerase III. *Genome Res.* 1997;7:1006-1019.
40. Grueneberg DA, Henry RW, Brauer A, et al. A multifunctional DNA-binding protein that promotes the formation of serum response factor/homeodomain complexes: identity to TFII-I. *Genes Dev.* 1997;11:2482-2493.
41. Palmer SJ, Tay ES, Santucci N, et al. Expression of Gtf2ird1, the Williams syndrome-associated gene, during mouse development. *Gene Expr Patterns.* 2007;7:396-404.
42. Bougel S, Renaud S, Braunschweig R, et al. PAX5 activates the transcription of the human telomerase reverse transcriptase gene in B cells. *J Pathol.* 2010;220:87-96.
43. Livide G, Epistolato MC, Amenduni M, et al. Epigenetic and copy number variation analysis in retinoblastoma by MS-MLPA. *Pathol Oncol Res.* 2012;18:703-712.
44. Polato F, Rusconi P, Zangrossi S, et al. DRAGO (KIAA0247), a new DNA damage-responsive, p53-inducible gene that cooperates with p53 as oncosuppressor. [Corrected]. *J Natl Cancer Inst.* 2014;106:dju053.
45. Wang Y, Wong MM, Zhang X, Chiu SK. Ectopic AP4 expression induces cellular senescence via activation of p53 in long-term confluent retinal pigment epithelial cells. *Exp Cell Res.* 2015;339:135-146.
46. Yasuda M, Tanaka Y, Nishiguchi KM, et al. Retinal transcriptome profiling at transcription start sites: A cap analysis of gene expression early after axonal injury. *BMC Genomics.* 2014;15:982.
47. Alfonso-Jaume MA, Mahimkar R, Lovett DH. Co-operative interactions between NFAT (nuclear factor of activated t cells) c1 and the zinc finger transcription factors Sp1/Sp3 and Egr-1 regulate MT1-MMP (membrane type 1 matrix metalloproteinase) transcription by glomerular mesangial cells. *Biochem J.* 2004;380:735-747.
48. Bikbova G, Oshitari T, Baba T, Yamamoto S. Altered expression of NF- κ B and Sp1 after exposure to advanced glycation end-products and effects of neurotrophic factors in ages exposed rat retinas. *J Diabetes Res.* 2015;2015:543818.
49. Donovan K, Alekseev O, Qi X, Cho W, Azizkhan-Clifford J. O-GlcNAc modification of transcription factor Sp1 mediates hyperglycemia-induced VEGF-A upregulation in retinal cells. *Invest Ophthalmol Vis Sci.* 2014;55:7862-7873.
50. Cubilla MA, Bermúdez V, Marquioni Ramella MD, Bachor TP, Suburo AM. Mifepristone, a blocker of glucocorticoid receptors, promotes photoreceptor death. *Invest Ophthalmol Vis Sci.* 2013;54:313-322.
51. Nader N, Chrousos GP, Kino T. Circadian rhythm transcription factor clock regulates the transcriptional activity of the glucocorticoid receptor by acetylating its hinge region lysine cluster: potential physiological implications. *FASEB J.* 2009;23:1572-1583.
52. Orlov SV, Kuteykin-Teplyakov KB, Ignatovich IA, et al. Novel repressor of the human FMR1 gene - identification of p56 human (GCC)(n)-binding protein as a krüppel-like transcription factor zF5. *FEBS J.* 2007;274:4848-4862.
53. Trimarchi JM, Firechild B, Verona R, Moberg K, Andon N, Lees JA. E2F-6, a member of the E2F family that can behave as a transcriptional repressor. *Proc Natl Acad Sci U S A.* 1998;95:2850-2855.
54. Koritschoner NP, Bocco JL, Panzetta-Dutari GM, Dumur CI, Flury A, Patrino LC. A novel human zinc finger protein that interacts with the core promoter element of a TATA box-less gene. *J Biol Chem.* 1997;272:9573-9580.
55. Nakamura H, Edward DP, Sugar J, Yue BY. Expression of Sp1 and KLF6 in the developing human cornea. *Mol Vis.* 2007;13:1451-1457.
56. Steketee MB, Oboudiyat C, Daneman R, et al. Regulation of intrinsic axon growth ability at retinal ganglion cell growth cones. *Invest Ophthalmol Vis Sci.* 2014;55:4369-4377.
57. Lim JQ, Lu J, He BP. Diva/BclB regulates differentiation by inhibiting NDPKB/Nm23H2-mediated neuronal differentiation in pc-12 cells. *BMC Neurosci.* 2012;13:123.
58. Fang J, Shaw PX, Wang Y, Goldberg JL. Krüppel-Like Factor 4 (KLF4) is not required for retinal cell differentiation. *eNeuro.* 2016;3:pii:ENEURO.0117-0115.2016.
59. Rowland BD, Peeper DS. KLF4, p21 and context-dependent opposing forces in cancer. *Nat Rev Cancer.* 2006;6:11-23.
60. Villarreal G Jr, Zhang Y, Larman HB, Gracia-Sancho J, Koo A, García-Cardena G. Defining the regulation of KLF4 expression and its downstream transcriptional targets in vascular endothelial cells. *Biochem Biophys Res Commun.* 2010;391:984-989.
61. Chen H, Privalsky ML. Cooperative formation of high-order oligomers by retinoid x receptors: an unexpected mode of DNA recognition. *Proc Natl Acad Sci U S A.* 1995;92:422-426.
62. Chen Y, Wang W, Liu F, Tang L, Tang R, Li W. 9-cis-retinoic acid improves sensitivity to platelet-derived growth factor-BB via RXR α and SHP-1 in diabetic retinopathy. *Biochem Biophys Res Commun.* 2015;465:810-816.
63. Cvekl A, Wang WL. Retinoic acid signaling in mammalian eye development. *Exp Eye Res.* 2009;89:280-291.

64. Janssen JJ, Kuhlmann ED, van Vugt AH, et al. Retinoic acid receptors and retinoid X receptors in the mature retina: Subtype determination and cellular distribution. *Curr Eye Res.* 1999;19:338-347.
65. Suzuki Y, Shimada J, Shudo K, Matsumura M, Crippa MP, Kojima S. Physical interaction between retinoic acid receptor and Sp1: mechanism for induction of urokinase by retinoic acid. *Blood.* 1999;93:4264-4276.
66. Bu Y, Gao L, Gelman IH. Role for transcription factor TFII-I in the suppression of SSeCKS/Gravin/Akap12 transcription by Src. *Int J Cancer.* 2011;128:1836-1842.
67. Kong X, Peng B, Yang Y, et al. P53 represses transcription of RING finger LIM domain-binding protein RLIM through Sp1. *PLoS One.* 2013;8:e62832.
68. Kong LM, Yao L, Lu N, et al. Interaction of KLF6 and Sp1 regulates basigin-2 expression mediated proliferation, invasion and metastasis in hepatocellular carcinoma. *Oncotarget.* 2016;7:27975-27987.
69. Okano J, Opitz OG, Nakagawa H, Jenkins TD, Friedman SL, Rustgi AK. The Krüppel-like transcriptional factors Zf9 and GKLf coactivate the human keratin 4 promoter and physically interact. *FEBS Lett.* 2000;473:95-100.
70. Miranda GA, Villalvazo M, Galic Z, et al. Combinatorial regulation of the murine RAG-2 promoter by Sp1 and distinct lymphocyte-specific transcription factors. *Mol Immunol.* 2002;38:1151-1159.
71. Wu CX, Zhao WP, Kishi H, et al. Activation of mouse RAG-2 promoter by Myc-associated zinc finger protein. *Biochem Biophys Res Commun.* 2004;317:1096-1102.
72. Chalepakis G, Gruss P. Identification of DNA recognition sequences for the PAX3 paired domain. *Gene.* 1995;162:267-270.
73. Choi WI, Jeon, BN, Yun CO, et al. Proto-oncogene FBI-1 represses transcription of p21CIP1 by inhibition of transcription activation by p53 and Sp1. *J Biol Chem.* 2009;284:12633-12644.